Journal of Applied Polymer Science

Determination of Temperatures of Polyamide 66 Directly from Near-Infrared Spectra

Chamathca P. S. Kuda-Malwathumullage, Gary W. Small
Department of Chemistry and Optical Science and Technology Center, University of Iowa, Iowa City, Iowa 52242
Correspondence to: G. W. Small (E-mail: gary-small@uiowa.edu)

ABSTRACT: The commercial importance of polyamides (PAs) motivates the development of chemical analysis tools for use in characterizing their structure and properties. Near-infrared (IR) spectroscopy offers advantages in this regard because of its simplicity of sample preparation and compatibility with sample thicknesses on the order of millimeters. For applications in which the measurement of sample temperature is difficult with a conventional probe, the work presented here demonstrates the ability to determine the temperature of PA 66 directly from its near-IR spectrum. Temperature-induced changes in spectral shape in the 4000–5000 cm^{-1} region are extracted through application of the discrete wavelet transform, and the resulting preprocessed spectra are submitted to partial least-squares regression to construct predictive models for temperature. These models are tested across different samples of PA 66 and over a time span of 7 weeks. Errors in predicted temperatures averaged 1.50°C over the range of 21–105°C. © 2014 Wiley Periodicals, Inc. J. Appl. Polym. Sci. **2014**, *131*, 40476.

KEYWORDS: spectroscopy; thermal properties; optical properties

Received 23 September 2013; accepted 17 January 2014
DOI: 10.1002/app.40476

INTRODUCTION

Nylon is the generic name given to a group of aliphatic polyamide (PA) polymers that are formed through condensation polymerization of a diamine with a dicarboxylic acid.[1] The United States, Canada and Mexico collectively produced 1,193 million pounds of these polymers in 2012.[2] Global production during this same period was estimated at more than 5,000 million pounds.[3]

Polyamide 66 (PA 66) is a subgroup of polymers synthesized by hexamethylenediamine and adipic acid monomers.[1] An important structural characteristic of PA 66 is the formation of hydrogen bonds between amide linkages. These hydrogen bonds hold together the polymer chains. PA 66 provides great rigidity, high mechanical strength, and durability, thereby making it one of the most widely used polymers in the world. Applications of PA 66 can be found in self-lubricating bearing parts, apparel, tires, zip ties, ropes, conveyer belts, carpets, electroinsulating elements, airbags, pipes, hoses, and in various machine parts.[4–7]

The commercial importance of PAs motivates the development of chemical analysis tools for use in characterizing their structure and properties. Among analysis methods, infrared (IR) spectroscopy is attractive because of the presence of numerous IR-active functional groups in the PA structure. As an example, mid-IR spectroscopy has been applied as a nondestructive tool to characterize PAs in several studies,[8–12] although strong absorption of light in this spectral region limits the technique to the analysis of thin polymer films.[13]

Previous studies have also applied near-IR spectroscopy to polymer characterization.[9,12–17] Spectral features in the near-IR region include combinations and overtones of the fundamental vibrational bands associated with C—H, O—H, and N—H bonds. The technique is nondestructive, requires little to no sample preparation, and is compatible with polymer samples of considerable thickness (e.g., in the millimeter range). However, the relatively weak and highly overlapped spectral features in the near-IR region complicate quantitative determinations, as a single wavelength or single spectral band can rarely be used alone for the implementation of a successful quantitative calibration. This factor demands the use of multivariate data analysis techniques when quantitative methods are developed from near-IR spectra.[18]

Among previous studies, Foster et al.[9] documented the use of near-IR spectral bands to study polymers such as PAs, polyethylenes, and polyisobutylenes. In this work, band assignments in the near-IR combination and overtone regions were included. Orendroff et al.[12] used near-IR spectroscopy to evaluate the effects of water and temperature on conformational order in PA thin films. Ghebremeskel et al.[16] used near-IR spectroscopy to study specific interactions in polymer blends, and Rodgers and

© 2014 Wiley Periodicals, Inc.

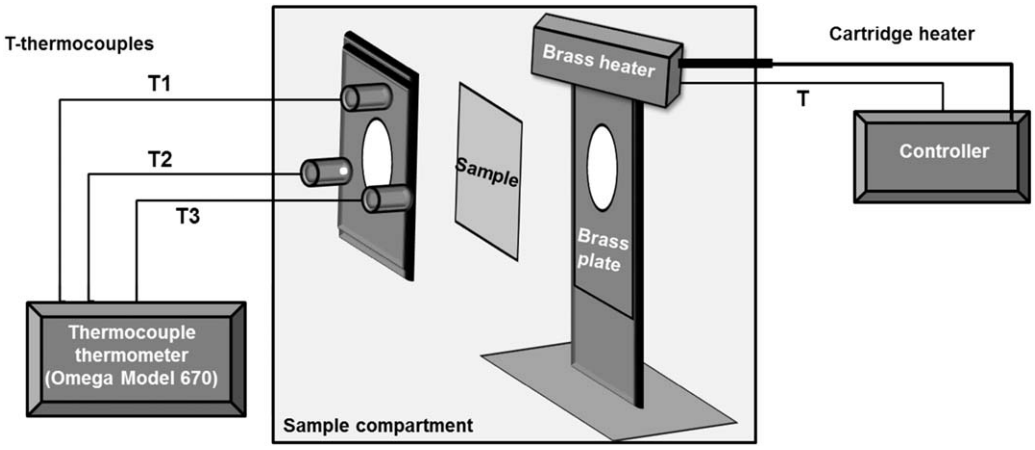

Figure 1. Schematic diagram of the custom-made brass heater used to obtain desired temperatures of the PA samples.

Lee used near-IR measurements to investigate the structural properties of PA 66 carpet yarns.[17] Wu et al.[14] studied the structural properties of amorphous PAs using two-dimensional near-IR spectroscopy, and Witschnigg et al.[19] applied near-IR measurements to polypropylene nanocomposites for the prediction of properties such as Young's modulus.

The research presented here extends the capabilities of near-IR spectroscopy to the quantitative prediction of physical properties of PA 66. In this work, the ability to determine the temperature of a PA 66 sample is demonstrated through a direct near-IR transmission measurement. The motivation for this work is to develop methods to predict the temperature of a polymer material directly from its near-IR spectrum, thereby providing a temperature measurement in applications in which it is inaccurate or inconvenient to determine the temperature with a conventional probe such as a thermocouple thermometer. Partial least-squares (PLS) regression[20] is used to develop calibration models to determine the temperature of a given piece of PA 66 directly from its near-IR spectrum. The prediction performance of these temperature models is assessed for robustness with time and the ability to predict temperatures across different sheets of PA 66.

EXPERIMENTAL

Apparatus and Reagents

The spectral data collection described here was performed with a Bruker Vertex 70 Fourier transform (FT) spectrometer configured with a tungsten–halogen lamp source, calcium fluoride beam splitter, and liquid nitrogen-cooled indium antimonide detector (Bruker Optics, Billerica, MA). A low-pass filter (OCLI, Santa Rosa, CA) was used to restrict the light beyond 5000 cm^{-1}, and a 6.3% neutral density filter (Rolyn Optics, Covina, CA) was used to attenuate the source intensity to prevent detector saturation. The same optical configuration was used during the collection of open-beam background spectra and during the measurement of the PA 66 samples. The beam diameter at the focal point of the sample compartment was 10 mm.

A custom-made brass heater was used to control the temperature of the PA samples during the spectroscopic measurements. A schematic of this device is presented in Figure 1. A cartridge heater (McMaster-Carr, PN3618K211) enclosed in a block of brass (89 mm × 51 mm × 38 mm) was used as the heating element for the sample, and two brass plates were mounted on two metal sample holder plates to increase the thermal conductivity of the assembly. The PA sample was sandwiched between the two sample holder plates. Three points of contact were made on one brass plate to input the three T-type thermocouples (5TC-GG-T-20–72; Omega Engineering, Stamford, CT) used to obtain the temperature of the sample at a given time. An Omega (CN7500 series; Omega Engineering) temperature controller was used to set the temperature of the cartridge heater to a desired value.

An Omega Model 670 digital thermocouple thermometer (Omega Engineering) equipped with T-type thermocouples was used to obtain temperature measurements. A Mettler AE200 analytical balance (Mettler-Toledo, Columbus, OH) was used to obtain the weight measurements of the pieces of PA 66. A Fisher Scientific Isotemp Model 655G oven (Fisher Scientific, Pittsburgh, PA) and a glass desiccator equipped with drierite (W.A. Hammond Drierite, Xenia, OH) were used for drying purposes.

Procedures

Commercially obtained PA 66 samples (McMaster-Carr, Elmhurst, IL) were used in this analysis. Four pieces of PA 66 (A, B, C, and D) were used in the spectral data collection. Each of these samples was obtained from a different sheet of the material. The average dimensions of the PA pieces were 35.00 × 35.00 × 0.40 ± 0.01 mm, and the average weight was 0.7215 ± 0.0001 g.

To build calibration models to relate spectral intensities to reference temperatures, a set of 72 spectra were collected using PA Piece A over a temperature range from room temperature (~21.0°C) to 105.0°C. This corresponded to three consecutive replicate spectra collected at 24 different temperature levels between 21.0 and 105.0°C. To assess the long-term predictive ability of the temperature models, 10 sets of spectra were collected using PA Pieces B, C, and D over the same temperature

Table I. Summary of Spectral Collection Protocol

Dataset	PA 66 piece used	Number of samples/ spectra collected[a]	Time since calibration (weeks)
Calibration	A	24/72	0
Prediction set 01 (PS01)	D	15/45	0.5
Prediction set 02 (PS02)	D	14/42	1.5
Prediction set 03 (PS03)	B	14/42	2.0
Prediction set 04 (PS04)	C	14/42	3.0
Prediction set 05 (PS05)	C	14/42	3.0
Prediction set 06 (PS06)	B	13/39	3.5
Prediction set 07 (PS07)	D	14/42	3.5
Prediction set 08 (PS08)	B	14/42	5.0
Prediction set 09 (PS09)	C	14/42	6.0
Prediction set 10 (PS10)	D	13/39	7.0

[a] A sample corresponds to one specific setting of the temperature controller.

range over a period of 7 weeks. The datasets collected are summarized in Table I.

All calibration and prediction spectra were obtained with dry PA 66. Each PA piece used in the data collection was dried in the oven to remove any moisture before the experiment. Weight measurements were obtained both before and after the spectral collection to verify that dry conditions were maintained. The brass heater described previously was used to heat the sample to a given temperature. The temperatures used during the spectral collection were randomized to minimize the correlation of temperature with time. Similar randomization procedures were used during the collection of the calibration and prediction data.

Open-beam air spectra were used as backgrounds in the calculation of absorbance spectra of the samples. For a given spectral collection session, eight warm-up air spectra were collected at the beginning of the day, and six air spectra were collected at the end of the day. The average of the 14 air spectra was used as the background in computing absorbance spectra of the PA samples measured during the corresponding data collection session.

The raw data consisted of 256 coadded double-sided interferograms containing 14,220 points collected at every zero crossing of the helium–neon reference laser (15800.45 cm^{-1}) with a nominal spectral resolution of 4 cm^{-1} and an aperture setting of 6 mm. All interferograms were converted to single-beam spectra with a point spacing of 1.9288 cm^{-1} by applying two levels of zero filling, Blackmann-Harris 3-term apodization and Mertz phase correction. The Fourier processing was performed with the Opus software (Version 6.5; Bruker Optics) controlling the spectrometer. After Fourier processing, single-beam spectra were reduced to the range of 5000–4000 cm^{-1}. Further calculations were performed with Matlab (Version 7.4; The Mathworks, Natick, MA) on a Dell Precision 670 computer (Dell Computer Corp., Round Rock, TX) operating under Red Hat Linux WS (Version 5.2; Red Hat, Raleigh, NC).

RESULTS AND DISCUSSION

Evaluation of Spectral Noise Levels

The quality of the spectra in the calibration and prediction sets was determined by the average root-mean-square (RMS) noise of the spectra in each dataset. To compute the noise in the spectra of the PA samples, ratios were taken of each pairwise combination of the three replicate spectra corresponding to a given temperature. The performance of the instrument was assessed by taking the ratio of each pairwise combination of the replicate air spectra for a given day. Noise spectra were converted to absorbance units (AUs) and fit to a third-order polynomial to remove systematic variation. In this study, the spectral region from 4800 to 4200 cm^{-1} was used to compute RMS noise values.

The average RMS noise values computed for PA (A) and air spectra (B) for each spectral dataset are displayed in Figure 2. The noise levels are consistent across the datasets. The higher noise values for the PA samples reflect the reduction in light intensity caused by absorption. Lower light levels under conditions of constant detector noise will result in higher spectral noise levels.

Near-Infrared Spectral Features and Thermal Behavior of PA 66

Figure 3 plots a spectrum in AUs over the range of 5000–4000 cm^{-1} for a 0.40-mm-thick piece of dry PA 66 at room temperature (21.0°C). This spectral region contains combination bands involving C—H, N—H, and O—H bonds. Previous studies regarding polymer characterization have identified characteristic

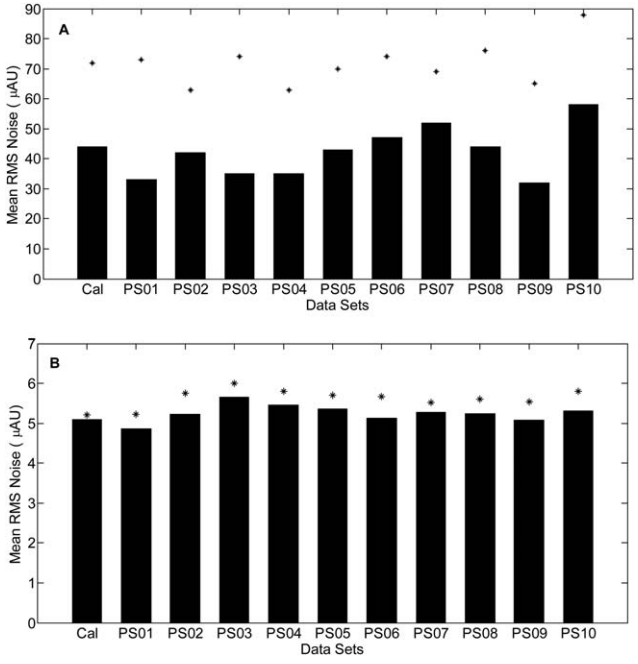

Figure 2. Average RMS noise values in units of microabsorbance (μAU) for (A) spectra of PA 66 and (B) air spectra for a given spectral collection. The asterisks represent one standard deviation from the average.

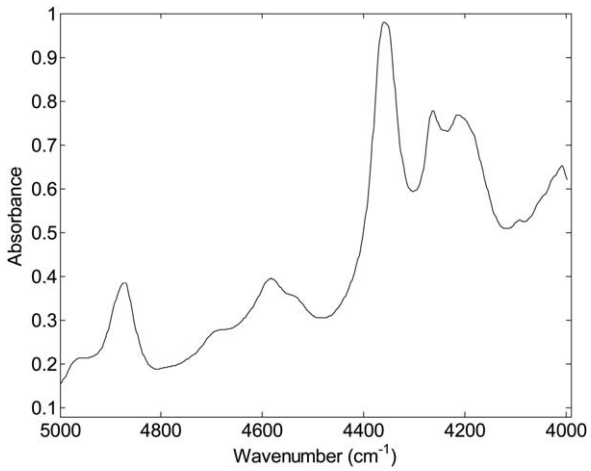

Figure 3. Absorbance spectrum of dry PA 66 (0.4 mm thickness) at room temperature relative to an open-beam air background.

peaks for PA in the near-IR region.[13–15] Combination bands of symmetric and asymmetric stretches of C—H bonds are located in the region of 4100–4400 cm^{-1}. The combination band of a fundamental N—H bending vibration and the Amide III fundamental vibration can be found at 4611 cm^{-1}. The third overtone of the Amide II fundamental vibration occurs at 4659 cm^{-1}, whereas the combination band of a fundamental N—H bend and the Amide II fundamental vibration can be found at 4877 cm^{-1}. Peaks related to amide linkages are expected to be broader than the other spectral features because the amide linkages are involved in hydrogen bonding between the individual PA chains.[13–15]

Polyamide 66 is not a good heat conductor. Linear expansion of PA 66 due to heating is negligible. Changes in temperature primarily affect the intermolecular hydrogen-bonding network that exists between the polymer chains. However, it is also observed that temperature changes can influence the structure of the hydrocarbon chains.[14,21] On heating of PA 66, combination peaks that arise due to hydrogen-bonded amide linkages as well as combination peaks that arise due to symmetric and asymmetric stretches of C—H bonds are expected to deviate.

Spectral Preprocessing Methods

In this study, the standard normal variate (SNV) transform[22] combined with the discrete wavelet transform (DWT)[23] were used to preprocess the PA absorbance spectra before submitting them to the PLS regression model. The preprocessing calculations were applied across the entire 5000–4000 cm^{-1} range.

The SNV method brings the spectra to a consistent scale by making the average and standard deviation of the spectral intensities equal to 0.0 and 1.0, respectively. The DWT implements a spectral decomposition that allows baseline variation and noise features to be suppressed.

Briefly, in the DWT, a selected wavelet function specified by a family type and order is scaled (stretched/compressed) and shifted over a discrete set of levels. Projection of the input signal (e.g., a near-IR spectrum) onto the wavelet functions yields a set of wavelet coefficients that describe a decomposition of the data. This decomposition is applied sequentially for a selected number of steps (levels). At each level of the decomposition, the DWT produces two sets of wavelet coefficients termed approximations and details. The approximations and details encode low- and high-frequency components of the data, respectively. After the first decomposition, the approximation obtained is further decomposed to produce a second set of approximations and details. This process can continue for as many levels of decomposition as desired.

Just as the input signal can be decomposed into the sets of approximations and details, the obtained wavelet coefficients can be used to reconstruct the signal. This is analogous to performing forward and inverse FTs. By a selective choice of which wavelet coefficients are used in reconstructing the signal, an operation analogous to digital filtering can be performed. This provides a flexible way to remove undesirable components from the data (e.g., baseline variation or noise).

The determination of how to use the DWT to remove undesired components from input data is typically performed through an optimization procedure. This optimization is performed once as an integral part of the calibration of the temperature model. Once chosen, the wavelet parameters remain static, and the subsequent application of the DWT to future data is straightforward and computationally fast.

In this work, optimization of the wavelet function (order), level of decomposition, and levels of details and approximations used in reconstructing the spectra was performed with a grid search. Spectra preprocessed with the SNV transform were used as inputs to the grid search. Details regarding the levels of each parameter studied will be given below in the discussion of the specific procedures used in generating the temperature models.

Near-Infrared Spectra of PA 66 at Different Temperatures

Figure 4 illustrates the spectra collected at different temperatures and preprocessed with the SNV and DWT methods. The Daubechies 6 (db6) wavelet function (i.e., the function of order 6 from the Daubechies family of wavelets) was used, implemented as five levels of decomposition and the use of the details in Levels 2, 3, and 4 only in reconstructing the spectra. Spectral features centered at 4350 and 4600 cm^{-1} show changes in intensity and peak position as the temperature changes. Combination peaks that arise due to symmetric and asymmetric stretches of C—H bonds are centered at 4350 cm^{-1}, whereas combination peaks that arise due to hydrogen-bonded amide linkages are centered at 4600 cm^{-1}. Thus, the observed spectral changes confirm the influence of temperature change both in the hydrogen-bonding network and the hydrocarbon chains in PA 66.

Assignment of Reference Temperatures

For the purpose of modeling, the reference temperature assigned to each PA piece was taken as the average of the readings of the three thermocouples depicted in Figure 1. An initial concern in adopting this procedure was the closer proximity of the heating element to thermocouple T_1 than to the other two thermocouples, T_2 and T_3. To investigate this issue, an alternate strategy of assigning the reference temperature to each spectrum was explored in which thermocouples T_1, T_2, and T_3 were weighted as 0.5, 0.25, and 0.25, respectively, in computing the

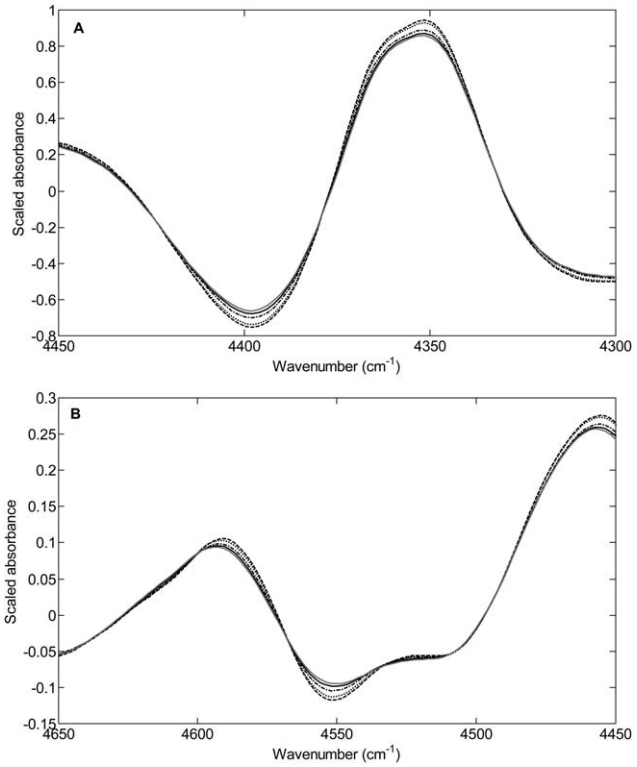

Figure 4. Preprocessed absorbance spectra of PA 66 collected at 21 (dashed), 40 (dotted), 60 (dash-dot), 80 (black solid), and 100°C (gray) over the wavenumber ranges (A) 4450–4300 cm^{-1} and (B) 4650–4450 cm^{-1}. Preprocessing was based on application of the SNV transform, followed by the DWT. The Daubechies 6 wavelet was used at five levels of decomposition, followed by the use of the details from Levels, 2, 3, and 4 only in reconstructing the spectra.

average. This method increased the influence of the T_1 reading on the computed average.

Linear regression was performed to compare sets of reference temperatures obtained with the two calculations. The slopes and intercepts differed by ~2%. When the 95% confidence intervals for the slope and intercept were considered, however, neither the slopes nor the intercepts were statistically different. On the basis of this evaluation, the two methods were judged to be equivalent. The method based on an unweighted average of the three thermocouples was adopted for its simplicity and used to establish the reference temperatures recorded for each collected spectrum.

Quantitative Modeling Procedures for Temperature Changes in PA 66

To model the temperature changes in PA 66 samples, PLS calibration models were generated from the computed absorbance spectra. As noted previously, these absorbance spectra were generated using single-beam PA spectra with respect to the average air spectrum obtained over the day of data collection. Absorbance spectra were preprocessed with the SNV and DWT methods before submitting them to the calibration model, and the calibration data matrix was mean-centered before the PLS calculation. A grid search protocol was used to optimize the wavelet parameters, as well as the spectral range submitted to the PLS calculation and the number of PLS latent variables (factors) used in the temperature model.

During this study, the grid search protocol used in the wavelet optimization included scanning the wavelet order from 2 to 8 for the db family (step size of 1). For each wavelet order investigated, the degree of decomposition was scanned from Level 3 to Level 8 (step size of 1). For each wavelet order and decomposition level studied, the best hierarchical combination of details to use in reconstructing the spectrum was evaluated. As an example, when the decomposition level was 5, the combinations of details evaluated were [2], [2, 3], [2, 3, 4], and [2, 3, 4, 5]. The Level 1 details and the last level approximation were never included in the grid search as these coefficients were never found to be useful.

For each combination of wavelet parameters studied, a further grid search was used to optimize the wavenumber range and the number of factors used in building the PLS model for temperature. The second grid search included scanning the wavenumber range from 4050 to 4950 cm^{-1} in steps of 25 cm^{-1} using window sizes from 300 to 800 cm^{-1} in steps of 25 cm^{-1}. For each wavenumber range investigated, models based on 1–10 PLS factors were computed.

A cross-validation (CV) procedure was used to validate the performance of each set of parameters related to the DWT, spectral range, and number of PLS factors. This procedure involved leaving out 10% of the calibration spectra with their replicate measurements and generating a temperature calibration model from the remaining spectra. The computed calibration model was then used to predict the temperatures corresponding to the withheld spectra, and the process was repeated until all spectra had been withheld once. A standard error of prediction (SEP) was pooled from the residuals of the predicted temperatures. This value is termed the cross-validated standard error of prediction (CV-SEP).

The minimum CV-SEP value was used as the criterion for selecting the optimal parameters for the calibration model. Once the optimal wavelet parameters and spectral range were established, a final selection of the number of latent variables was performed by assessing whether models with fewer latent

Table II. Summary of the Best PLS Calibration Models for Temperature Changes in PA 66

Wavenumber range (cm^{-1})	Number of factors	Preprocessing method	SEC (°C)	CV-SEP (°C)
4650–4300	3	SNV and DWT (db6, 5 [2, 3, 4])[a]	0.61	0.75
4800–4500	5	None	0.50	0.68

[a] Notation is wavelet family and order of wavelet function, number of levels of decomposition, and the levels of details used in the reconstruction of the spectrum.

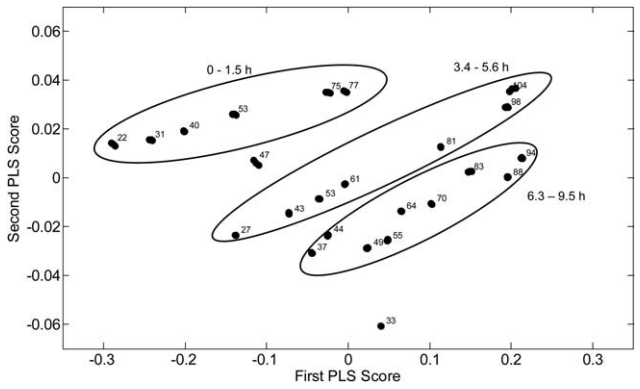

Figure 5. Partial least-squares scores along the first two latent variables for the preprocessed spectra of PA 66 used in the calibration model. Data labels are the corresponding sample temperatures. Scores are plotted for the three replicate spectra collected at each temperature setting. The two PLS factors account for greater than 99% of the data variance. As shown by the superimposed ellipses, temperature information appears to be encoded in three prominent bands of increasing temperature from the lower left to the upper right of the figure. These three bands seem to be clustered according to the time of data collection, as indicated by the elapsed time ranges (in hours relative to the start of data collection) placed next to each ellipse.

variables than that producing the minimum CV-SEP were statistically equivalent (i.e., not statistically different). An *F*-test at the 95% level was used to make this determination.

Calibration Models for Temperature Changes in PA 66

Calibration models were generated for temperature variations in PA 66 using PLS regression. Models were developed separately for preprocessed (i.e., application of the SNV and DWT procedures) and raw PA absorbance spectra. For models built with raw absorbance spectra, the same grid search described above was used for the optimization of the wavenumber range

Table III. Prediction Performance of PLS Calibration Models for Temperature Changes in PA 66

Dataset	PA 66 piece used	SEP for preprocessed spectra (°C)	SEP for raw spectra (°C)
Calibration[a]	A	0.75	0.68
Prediction set 01 (PS01)	D	1.15	2.95
Prediction set 02 (PS02)	D	1.61	1.25
Prediction set 03 (PS03)	B	0.84	2.37
Prediction set 04 (PS04)	C	2.65	6.40
Prediction set 05 (PS05)	C	1.87	16.9
Prediction set 06 (PS06)	B	1.03	15.8
Prediction set 07 (PS07)	D	1.49	11.9
Prediction set 08 (PS08)	B	0.70	9.55
Prediction set 09 (PS09)	C	2.16	16.8
Prediction set 10 (PS10)	D	1.50	18.2

[a] Results given for the calibration data are values of CV-SEP.

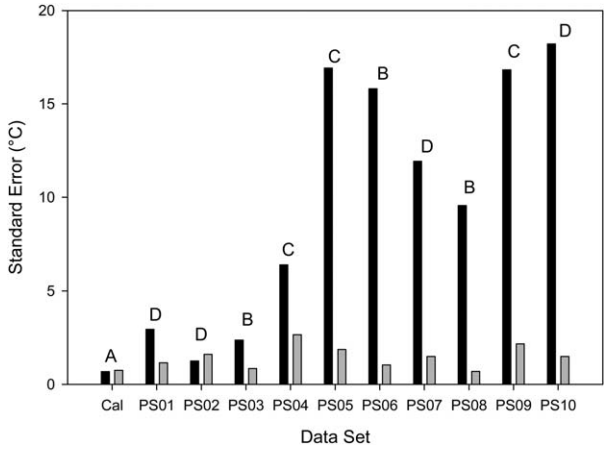

Figure 6. Prediction performance of PLS calibration models for temperature changes in PA 66. Values of SEP are plotted for the prediction sets, whereas CV-SEP is displayed for the calibration data. The left (black) and right (gray) bars within each group correspond to the models based on raw and preprocessed absorbance spectra. The labels above each group of bars correspond to the piece of PA 66 used in the data collection. The models based on preprocessed spectra clearly outperform those based on raw absorbance spectra. When the results based on preprocessed spectra are considered, PA 66 Piece C consistently produces the highest prediction errors.

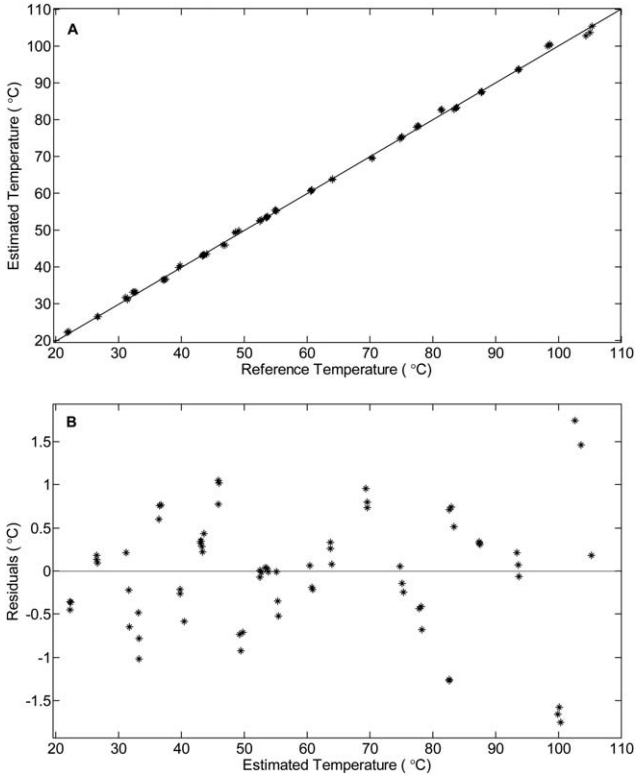

Figure 7. Correlation (A) and residual (B) plots for the calibration data used to build the model for temperature changes in PA 66. Piece A was used. The solid lines in Panels A and B denote perfect correlation between estimated and reference temperatures and residuals of 0.0°C, respectively. Both plots show a good correlation and randomly scattered unbiased residuals.

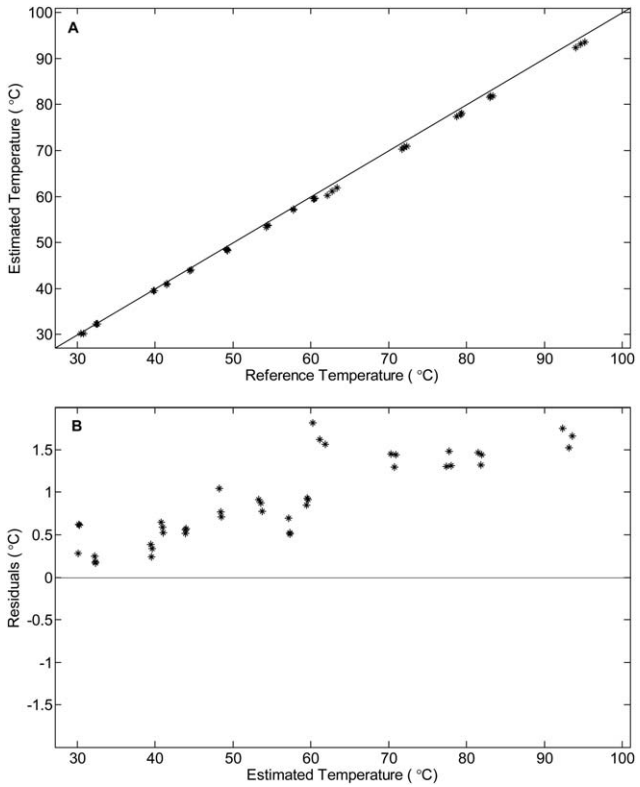

Figure 8. Correlation (A) and residual (B) plots for prediction set 6 (PS06) for temperature changes in PA 66. The solid lines in Panels A and B denote perfect correlation between estimated and reference temperatures and residuals of 0.0°C, respectively. Piece B was used in this prediction, and the duration was 3.5 weeks after calibration. A slight bias is observed in both the correlation and residual plots.

submitted to the PLS calculation and the number of PLS factors used in the final model.

These models are summarized in Table II. The wavenumber ranges, number of PLS latent variables, and values of the standard error of calibration (SEC) and CV-SEP are listed in the table. The SEC is the standard error in predicted temperatures achieved with the calibration data when all spectra were included in the calculation of the model.

The optimal wavenumber range for preprocessed spectra was 4650–4300 cm^{-1} with three PLS factors used to construct the model. The DWT preprocessing used the db6 wavelet function at five levels of decomposition, with Levels 2, 3, and 4 only used for reconstructing the spectra. These are the parameters used to preprocess the spectra displayed in Figure 4. The best calibration model gave a CV-SEP value of 0.75°C. By comparison, the optimal wavenumber range for raw spectra was 4800–4500 cm^{-1} with five PLS factors. The best calibration model gave a CV-SEP value of 0.68°C.

Figure 5 is a PLS score plot that illustrates the data variance encompassing the preprocessed PA spectra used to compute the calibration model. Scores along the first two PLS factors are plotted. The first PLS factor explains about 97% of the spectral variance. Spectra collected at a given temperature tend to cluster together. However, as shown by the superimposed ellipses, temperature information is encoded in three prominent bands of increasing temperature from the lower left to the upper right of the figure. As shown by the time ranges indicated for each ellipse (elapsed time relative to the start of data collection), these three bands are clustered according to the time of data acquisition. Some time-dependent spectral drift effects are thus embedded in the data.

Prediction Performance of Temperature Models for PA 66

The long-term prediction performance of the calibration models was assessed using 10 prediction sets of PA 66 spectra collected over a period of 2 months. These results are summarized in Table III. The prediction performance of the calibration model based on the raw absorbance spectra was poor, with SEP values exceeding 6°C after 3 weeks. The calibration model based on preprocessed spectra gave good prediction results with SEP values ranging from 0.70 to 2.65°C and averaging 1.50°C. Moreover, the model based on preprocessed spectra was able to predict temperatures across different sheets of PA 66. Piece C gave the highest SEP values (average SEP of 2.23°C) when compared with the other pieces of PA 66 (average SEP of 0.857 and 1.44°C for Pieces B and D, respectively).

Figure 6 is a bar chart that presents the CV-SEP value for the calibration data and the SEP values for the prediction sets.

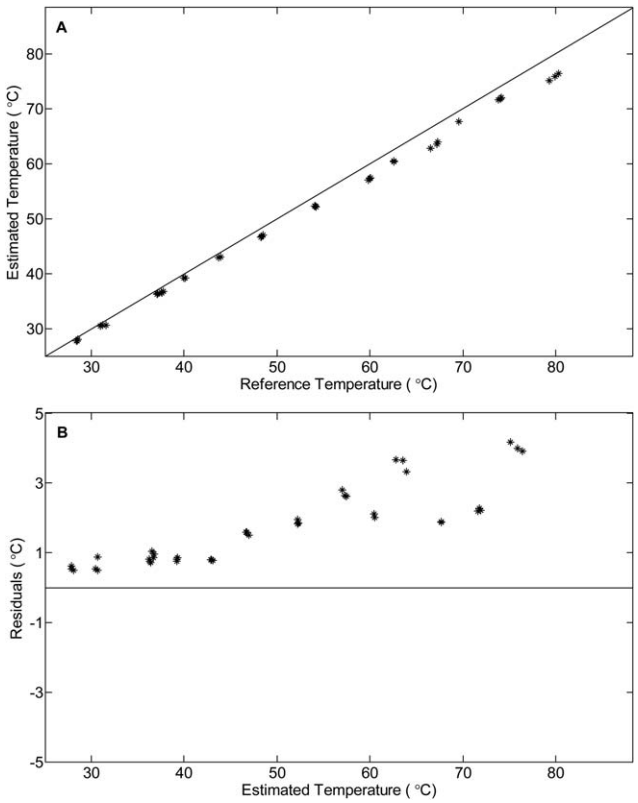

Figure 9. Correlation (A) and residual (B) plots for prediction set 4 (PS04) for temperature changes in PA 66. The red lines in Panels A and B denote perfect correlation between estimated and reference temperatures and residuals of 0.0°C, respectively. Piece C was used in this prediction, and the duration was 3.0 weeks after calibration. Increased bias is noted in both the correlation and residual plots relative to the results for Piece B in Figure 8.

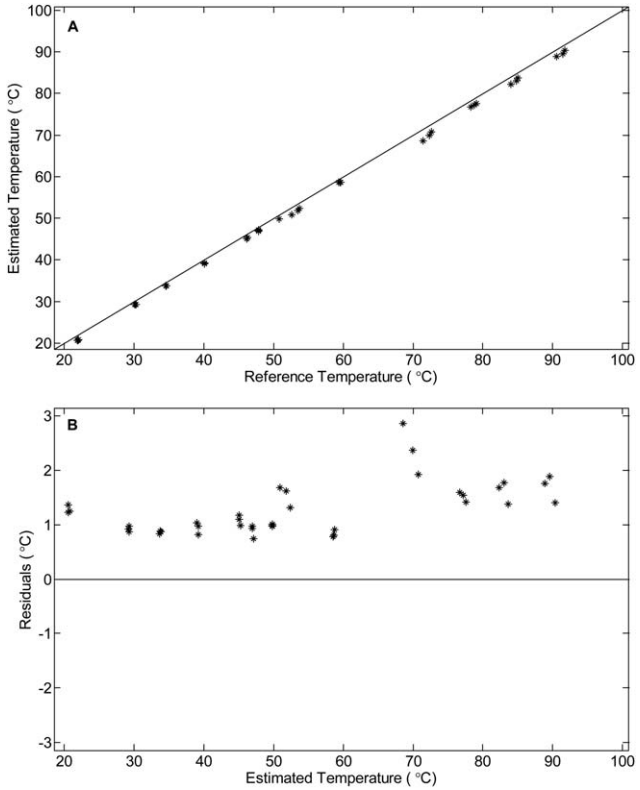

Figure 10. Correlation (A) and residual (B) plots for prediction set 10 (PS10) for temperature changes in PA 66. The solid lines in Panels A and B denote perfect correlation between estimated and reference temperatures and residuals of 0.0°C, respectively. Piece D was used in this prediction, and the duration was 7.0 weeks after calibration. Less bias is noted in the correlation and residual plots relative to the results for Piece C in Figure 9.

Paired bars are included for the models computed with and without spectral preprocessing, and the groups of bars are labeled according to the piece of PA 66 used. No significant degradation of performance in the calibration model based on preprocessed spectra is noted over time. The model based on raw absorbance data degrades noticeably as the time since calibration increases. However, the specific piece of PA 66 has a clear influence on the temperature prediction. Within the results for a given PA piece, however, there is no obvious degradation in model performance with time.

Figure 7 presents correlation and residual plots for the calibration data used to build the model for temperature changes in PA 66. The figure is derived from the preprocessed spectra. Excellent correlation between predicted and observed temperatures is observed throughout the temperature range. The residual plot appears randomly scattered with no obvious indicators of deficiency in the model.

Figures 8–10 present similar correlation and residual plots for prediction sets PS06, PS04, and PS10, respectively. These figures are also based on the preprocessed absorbance spectra. The results in Figures 8–10 correspond to PA Pieces B, C, and D, respectively. The prediction sets displayed in Figures 8–10 also span the times of 3.5 (PS06), 3.0 (PS04), and 7.0 (PS10) weeks removed from the calibration data. The results presented for Piece C in Figure 9 represent the worst prediction data obtained in the study (SEP = 2.65°C).

Although the predictions are very successful when placed into the context of the ~80°C temperature range of the data, some bias is observed with each set of predicted values. This appears to be primarily related to the sheet of PA 66, suggesting that a more robust model may require the representation of different sheets of polymer in the calibration data.

CONCLUSIONS

In this research, the methodology was successfully developed for the prediction of the temperatures of samples of PA 66 directly from their near-IR spectra. This approach was based on the occurrence of temperature-induced changes in the intensity and position of spectral bands associated with hydrogen-bonded amide groups and hydrocarbon chains. This methodology provides a way to measure sample temperatures when the use of conventional temperature probes is undesirable.

A signal processing method based on the combination of the SNV and DWT procedures was found to be successful in standardizing the spectra before they were submitted to quantitative models based on PLS regression. These preprocessing steps allowed the small deviations observed in near-IR spectra of PA 66 as a function of temperature to be extracted reliably.

The long-term prediction performance of the temperature models was assessed using 10 prediction sets of PA 66 spectra at different temperatures spanning a period of 7 weeks. The temperature model based on raw absorbance spectra gave very high SEP values (>6°C) after prediction set PS04 (3 weeks since calibration), whereas the model based on preprocessed spectra provided improved SEP values (0.697–2.65°C) with time.

The use of wavelet functions to standardize the spectra significantly improved the performance of the temperature model with time and also improved the prediction performance across different sheets of PA 66. Temperature models based on preprocessed spectra gave similar SEP values across the different polymer sheets. However, PA Piece C gave high SEP values (average SEP = 2.23°C) when compared with the other three PA pieces (average SEP = 1.19°C). This might be due to the inhomogeneous nature of different sheets of polymer at a microscopic level.

In principle, these temperature models are not limited to PA 66, but could be applied to other PAs as well because all the PA polymers contain the same basic chemical structure. This represents a potential area for further investigation.

ACKNOWLEDGMENTS

The authors thank Mike Estenson and Frank Turner for their help in the design and construction of the temperature-controlled sample holder used in this research.

REFERENCES

1. Braun, E.; Levin, B. C. *Fire Mater.* **1987**, *11*, 71.
2. American Chemistry Council. U.S. Resin Production and Sales 2012 vs. 2011; **2013**. Available at: http://www.

americanchemistry.com/Jobs/EconomicStatistics/Plastics-Statistics/Production-and-Sales-Data-by-Resin.pdf.

3. Production of Man-Made Fiber in Taiwan, Japan, Korea, USA, Mainland China for the Whole Year of 2012; Taiwan Man-Made Fiber Industries Association, **2013**. Available at: http://www.tmmfa.org.tw/file/1474_20130628014812.pdf.
4. Library, P. D. Handbook of Plastics Joining: A Practical Guide; William Andrew: New York, **1997**.
5. Olabisi, O. Handbook of Thermoplastics; Marcel Dekker: New York, **1997**.
6. Ghosh, P. Polymer Science and Technology: Plastics, Rubbers, Blends and Composites; Tata McGraw-Hill: New Delhi, **2002**.
7. Gooch, J. W. Encyclopedic Dictionary of Polymers; Springer: New York, **2011**; Vol. *1*.
8. Mohan, J. Organic Spectroscopy: Principles and Applications, 2nd ed.; Alpha Science International: Oxford, UK, **2002**.
9. Foster, G. N.; Row, S. B.; Griskey, R. G. *J. Appl. Polym. Sci.* **1964**, *8*, 1357.
10. Charles, J.; Ramkumar, G. R.; Azhagiri, S.; Gunasekaran, S. *E-J. Chem.* **2009**, *6*, 23.
11. Dasgupta, S.; Hammond, W. B.; Goddard, A., III. *J. Am. Chem. Soc.* **1996**, *118*, 12291.
12. Orendroff, C. J.; Huber, D. L.; Bunker, B. C. *J. Phys. Chem. C* **2009**, *113*, 13723.
13. Camacho, W.; Valles-Liuch, A.; Ribes-Greus, A.; Karlsson, S. *J. Appl. Polym. Sci.* **2003**, *87*, 2165.
14. Wu, P.; Yang, Y.; Siesler, H. W. *Polymer* **2001**, *42*, 10181.
15. Lachenal, G. *Vib. Spectrosc.* **1995**, *9*, 93.
16. Ghebremeskel, Y.; Fields, J.; Garton, A. *J. Polym. Sci. Part B: Polym. Phys.* **1994**, *32*, 383.
17. Rodgers, J. E.; Lee, S. *Text. Res. J.* **1991**, *61*, 531.
18. Small, G. W. *Trends Anal. Chem.* **2006**, *25*, 1057.
19. Witschnigg, A.; Laske, S.; Kracalik, M.; Feuchter, M.; Pinter, G.; Maier, G.; Märzinger, W.; Haberkorn, M.; Langecker, G. R.; Holzer, C. *J. Appl. Polym. Sci.* **2010**, *117*, 3047.
20. Haaland, D. M.; Thomas, E. V. *Anal. Chem.* **1988**, *60*, 1193.
21. Lewin, M. Handbook of Fiber Chemistry, 3rd ed.; CRC Press: Boca Raton, FL, **2007**.
22. Luypaert, J.; Heuerding, S.; Vander Heyden, Y.; Massart, D. L. *J. Pharm. Biomed. Anal.* **2004**, *36*, 495.
23. Jensen, A.; La Cour-Harbo, A. Ripples in Mathematics: The Discrete Wavelet Transform; Springer-Verlag: Heidelberg, **2001**.